



## Functionalized polymer microbubbles as new molecular ultrasound contrast agent to target P-selectin in thrombus



Bo Li<sup>a,b,c</sup>, Rachida Aid-Launais<sup>a,b</sup>, Marie-Noëlle Labour<sup>a,b</sup>, Alina Zenych<sup>a,b</sup>, Maya Juenet<sup>a,b</sup>, Christine Choqueux<sup>a,b</sup>, Véronique Ollivier<sup>a,b</sup>, Olivier Couture<sup>d</sup>, Didier Letourneur<sup>a,b</sup>, Cédric Chauvierre<sup>a,b,\*</sup>

<sup>a</sup> INSERM, U1148, Laboratory for Vascular Translational Science, CHU X. Bichat, Paris Diderot University, 46 Rue H. Huchard, 75018 Paris, France

<sup>b</sup> Institut Galilée, Paris 13 University, 99 Avenue JB Clément, 93430 Villetaneuse, France

<sup>c</sup> Key Laboratory of Biomaterials of Guangdong Higher Education Institute, Department of Biomedical Engineering, Jinan University, Guangzhou 510632, China

<sup>d</sup> Institut Langevin - Ondes et Images, ESPCI ParisTech, PSL Research University, CNRS UMR7587, INSERM U979, 1, Rue Jussieu, 75238 Paris, Cedex 05, France

### ARTICLE INFO

#### Keywords:

Polymer microbubbles  
Fucoidan  
P-selectin  
Molecular ultrasound imaging  
Thrombosis

### ABSTRACT

Thrombotic diseases rarely cause symptoms until advanced stage and sudden death. Thus, early detection of thrombus by a widely spread imaging modality can improve the prognosis and reduce mortality. Here, polymer microbubbles (MBs) made of degradable poly(IsoButylCyanoAcrylate) and functionalized with fucoidan (Fucoidan-MBs) were designed as a new targeted ultrasound contrast agent to image venous thrombus. The physicochemical characterizations demonstrate that the MBs with fucoidan surface exhibit a size of 2–6 μm and stability in suspension at 4 °C up to 2 months. MBs exhibit high echogenicity and could be completely burst under high destructive pulse. Flow chamber experiments on activated human platelets show a higher affinity of Fucoidan-MBs than control anionic MBs (CM-Dextran-MBs) under shear stress conditions. *In vivo* analysis by ultrasound and histological results demonstrate that Fucoidan-MBs are localized in rat venous thrombotic wall, whereas few CM-Dextran-MBs are present. In addition, the binding of Fucoidan-MBs in healthy vein is not observed. Collectively, Fucoidan-MBs appear as a promising functionalized carrier for ultrasound molecular imaging in thrombotic diseases.

### 1. Introduction

Thrombotic diseases, such as deep vein thrombosis, are often called “the silent killer” because they rarely cause symptoms until an advanced stage [1–3]. Early detection and treatment can improve the prognosis and reduce mortality. P-selectin, an adhesion molecule, mainly expressed on the surface of activated platelets and injured vascular endothelium, is involved in the pathophysiology of intraluminal thrombus formation and other cardiovascular diseases [4,5]. These features suggest that P-selectin can be an important target for molecular imaging of thrombosis or in acute and chronic cardiovascular diseases [6–8].

We have previously demonstrated that fucoidan, an abundant and cost-effective marine polysaccharide with sulfated chains, exhibits a high affinity for immobilized P-selectin *in vitro* [9,10]. <sup>99m</sup>Tc-fucoidan as a radiotracer has already proved *in vivo* to be able to detect thrombus and heart ischemia associated with the P-selectin overexpression in our

previous studies [11,12]. Recently, we have developed fucoidan functionalized core-shell polymer microcapsules and proved that they have high specific binding efficiency to P-selectin under flow conditions [13]. Moreover, fucoidan functionalized nano-/microparticles have also been developed as a molecular contrast agent to monitor thrombi by Magnetic Resonance Imaging (MRI) or Single-Photon Emission Computed Tomography (SPECT) imaging [14–16].

Compared to other imaging modalities, ultrasound imaging has numerous advantages, including comfortable, noninvasive, portable, low cost real-time imaging, lack of ionizing radiation and excellent safety profile [17,18]. Ultrasound imaging equipment is already present in most hospitals all around the world and even in private health centers. However, ultrasound image quality is limited by its poor contrast due to the low differences in acoustic characteristics of organs *in vivo*. The development and use of microbubbles (MBs) have redeemed this shortage tremendously [19–22]. Traditional MBs are mainly made up of albumin/lipid/surfactant shells and have not only been applied as

\* Corresponding author. INSERM, U1148, Laboratory for Vascular Translational Science, CHU X. Bichat, Paris Diderot University, 46 rue H. Huchard, 75018 Paris, France.

E-mail address: [cedric.chauvierre@inserm.fr](mailto:cedric.chauvierre@inserm.fr) (C. Chauvierre).

<https://doi.org/10.1016/j.biomaterials.2018.12.023>

Received 3 September 2018; Received in revised form 28 November 2018; Accepted 20 December 2018

Available online 23 December 2018

0142-9612/ © 2018 Published by Elsevier Ltd.

ultrasound agents, but also have been used in versatile biomedical applications including drugs, genes and drug-loaded nanoparticles targeted delivery [23,24]. Recently, polymeric shells MBs have received increasing attention due to their improved stability and some polymersomes have also been applied in drug controlled release at the target site under a specific stimulus such as ultrasound [25,26]. Poly (AlkylCyanoAcrylate) with long alkylcyanoacrylate monomers (for example, *n*-butyl, isobutyl, isohexyl and octyl) has been extensively investigated to design micro-/nanocarriers since the 80s [27,28]. The first Poly(ButylCyanoAcrylate) microbubbles called Sonavist<sup>®</sup> were manufactured by one-step process through adding the *n*-butyl-2-cyanoacrylate monomers into gas-water emulsion [29,30]. Palmowski et al. further synthesized streptavidin-coated PBCA microbubbles and investigated their physicochemical properties [31–33]. Subsequent studies proved that these microbubbles could be functionalized by conjugating with monoclonal antibodies that recognize receptor proteins involved in various diseases [34–36]. However, employing, for instance, biotin/streptavidin and antibodies limited their use in humans because of the costs and potential immunogenicity of streptavidin and antibodies. Recently, various bubbles using small peptides instead of antibodies for binding without using the biotin-streptavidin coupling strategy have already been developed to address these problems [37,38]. Among them, BR55, as the most potential targeted-MBs contrast agent, shows that it could be used to detect the prostate cancer or monitor breast and ovarian lesions in human clinical trials [39,40]. In the view of future clinical applications, MBs assembled by clinically approved polymers and suitable targeting ligands are interesting for clinical use and market requirements.

In this work, we report a new one-step process to obtain polysaccharide-coated poly(IsoButylCyanoAcrylate) (PIBCA) microbubbles. Among them, fucoidan functionalized microbubbles (Fucoidan-MBs) were considered as a targeted ultrasound molecular imaging probe for P-selectin. Targeting of Fucoidan-MBs was evaluated *in vitro* using flow chambers with activated human platelets. *In vivo* experiments performed in a FeCl<sub>3</sub>-induced thrombus rat model showed that Fucoidan-MBs were located in the thrombotic area but not in healthy rats, which confirms the ability of Fucoidan-MBs to specifically target P-selectin. These functionalized echogenic microbubbles appear as new tools for imaging at molecular level cardiovascular events in which P-selectin is overexpressed.

## 2. Materials and methods

**Materials:** Dextran 70, anionic CarboxyMethyl-Dextran 40 (CM-Dextran), FITC-CarboxyMethyl-Dextran 40 (FITC-CM-Dextran) and cationic 2-DiEthylAminoethyl-Dextran 70 (DEAE-Dextran) were provided from TdB Consultancy (Uppsala, Sweden). Fucoidan (Mn = 18 kDa/Mw = 104 kDa) was obtained from Algues & Mer (Ouessant, France). Isobutylcyanoacrylate (IBCA) monomers were purchased by ORAPI (Saint Vulbas, France). Methylene blue hydrate was purchased from Sigma-Aldrich. Chromatography was obtained from GE Healthcare. Mouse anti-human CD62P-FITC and mouse IgG1-FITC Isotype Control were provided from Beckman Coulter (Villepinte, France). Fibrillar type I collagen Horm<sup>®</sup> was obtained from Takeda (Linz, Austria). 24-, 96-Well Cell Culture Plates (Costar) were obtained from Corning Incorporated. PPACK tubes were purchased from Cryopep (Montpellier, France). Flow chambers (Vena8 Fluoro+) were provided from Cellix Ltd (Dublin, Ireland).

**Synthesis of Microbubbles:** Poly(IsoButylCyanoAcrylate) (PIBCA) shelled air-containing microbubbles (MBs) were prepared by modification of established emulsion polymerization process as described by Palmowski et al. [33]. Briefly, 700 µL of IBCA monomer was loaded in a 1 mL plastic syringe, injected into 50 mL of an aqueous solution of 1% Tween 20 at pH 2.5 via a catheter at a constant flow rate of 5 mL h<sup>-1</sup>, and dispersed at 20,000 rpm for 60 min with a homogenizer (ULTRA-TURRAX<sup>®</sup>, IKA, Germany). The syringe pump (AL-300, World Precision

Instruments, Florida, USA) was used to control flow rate. The resulting microbubble suspension was then washed three times by centrifugation (500 rpm, 20 min, 5702RH centrifuge Beckman Coulter, Villepinte, France) to obtain the monodispersed bubble populations and to remove the polymeric scrap. Subsequently, the resulted emulsion was placed into a separatory funnel overnight, and the aqueous layer was removed. The microbubbles layer was redispersed in 30 mL of 0.02% Tween 20 for storage at 4 °C. To prepare polysaccharide functionalized microbubbles (Dextran-MBs, DEAE-Dextran-MBs, CM-Dextran-MBs and Fucoidan-MBs), 500 mg of corresponding polysaccharides were dissolved in an aqueous solution before IBCA introduction. For Rhodamine B loaded CM-Dextran-MBs and Fucoidan-MBs (CM-Dextran-RhoB-MBs and Fucoidan-RhoB-MBs, respectively), 1 mg of Rhodamine B was added into an aqueous solution before synthesis. FITC-CM-Dextran-MBs and FITC-Fucoidan-MBs were obtained by using 10 mg of FITC-CM-Dextran mixed with 490 mg of CM-Dextran and 10 mg of FITC-Fucoidan mixed with 490 mg of Fucoidan, respectively. Rhodamine B loaded FITC-CM-Dextran-MBs and FITC-Fucoidan-MBs were prepared by combining two protocols.

**Microbubbles Size and Zeta Potential Analysis:** The size range of microbubbles was determined using a Mastersizer 3000 (Malvern Instruments, UK) equipped with a Hydro SM sample dispersion unit. A suspension of microbubbles was dispersed into 0.02% Tween 20 solution and stirred at 1500 rpm for 1 min before an examination. Zeta potential (ζ) of the microbubbles was measured with samples diluted into electrolyte solution (1 × 10<sup>-3</sup> M KCl & 0.02% Tween 20) using electrophoretic light scattering apparatus (Nano ZS, Malvern Instruments, UK) at 25 °C. All the measurements were performed at least three times.

**Environmental Scanning Electron Microscopy (ESEM) and Scanning Electron Microscopy (SEM):** The surface morphology of microbubbles was imaged using an ESEM apparatus (Philips XL30 ESEM-FEG, Amsterdam, Netherlands) and SEM apparatus (JSM-IT100, Jeol, Japan). The interaction of Fucoidan-MBs with activated platelets on an *ex vivo* platelets-rich thrombus was also visualized using ESEM. Briefly, to obtain the *ex vivo* platelets-rich thrombus, the blood was collected in citrate tubes and then centrifuged at 120 G for 15 min. Plasma rich in platelets (PRP) was collected and distributed in small glass tubes (370 µL). To activate platelets, calcium chloride was added (7 µL at 1 M) and the tubes were incubated at 37 °C for 1 h. The platelet-rich thrombus was detached from the walls of the glass tubes and then transferred to a 96-well plate where it was put in contact with Fucoidan-MBs for 5 min. After several rinses with 0.9% NaCl, the thrombus was fixed at 4% paraformaldehyde for 24 h and then rinsed for visualization by ESEM.

The binding of Fucoidan-MBs on the luminal thrombus of inferior vena cava was observed using ESEM. Briefly, we performed an inferior vena cava thrombus rat model induced by ferric chloride (FeCl<sub>3</sub>), and injected Fucoidan-MBs. The rat was then euthanized and the inferior vena cava with thrombus was picked up and fixed in 4% paraformaldehyde for 24 h and rinsed in saline. The inferior vena cava was opened longitudinally on the top to observe the thrombus by ESEM.

**Confocal imaging:** Microbubbles were imaged using Zeiss LSM 780 confocal microscope fitted with 63× objective. Microbubbles were detected using rhodamine B and polysaccharides with FITC-Fucoidan and FITC-CM-Dextran.

**Quantification of Fucoidan content:** The amount of fucoidan in microbubbles was determined by methylene blue staining of sulfated polysaccharides [41]. Several 1 × 1 cm square chromatography paper were placed in 24-well plate. The solution was cautiously added dropwise at the center of these squares, 2 µL for each drop; the next portions were dropped on the same point after drying off the last drop in the oven (Jouan, France) for 10 min at 50 °C. The filter papers with loaded sample drops were kept in the oven overnight at 50 °C, dried thoroughly and then treated with a mixture of methanol and acetone (6:4) for 3 min. Fucoidan spots on filter paper were visualized after

10 min at room temperature in staining solution containing 50 mM HCl and 0.1% (w/w) methylene blue in a mixture of methanol/acetone/water (6:4:15). The filter paper was washed several times with a mixture of acetic acid/methanol/acetone/water (5:6:4:75) to remove the excess of methylene blue. Images were taken, and filter paper squares were put into 1.5 mL Eppendorf centrifuge tubes with 0.5 mL of methanol containing 2% SDS during 15 min at 50 °C. A volume of 0.1 mL of this extract was transferred into 96-well plate, and absorbance was determined at 663 nm by infinite<sup>®</sup> 200 PRO (TECAN, Switzerland). The series of filter paper squares containing stained standard solution spots was obtained by adding 5 drops (10  $\mu$ L) of different concentration of fucoidan or CM-Dextran solutions (0.5, 0.25, 0.125, 0.0625 and 0.3125 mg mL<sup>-1</sup>) to each filter paper. The relative absorbance ( $\Delta$ abs) of fucoidan - methylene blue complex at A<sub>663</sub> nm was expressed as [abs (fucoidan) - abs (CM-Dextran)]. Fucoidan content was plotted against the  $\Delta$ abs for the regression line. For MBs samples, 3  $\times$  10<sup>8</sup> Fucoidan or CM-Dextran microbubble suspension was placed into a separatory funnel overnight, and the aqueous layer was removed to eliminate free fucoidan. The clot of microbubbles was totally hydrolysed by mixing with alkaline solution (0.1 N NaOH and 0.02% Tween 20) overnight, and the resulted solution was added dropwise on filter paper square.

**Flow Chamber Experiments:** Platelet dynamic binding experiments were performed according to our previous methods [13]. Briefly, Vena8 Fluoro + channels were coated with 50  $\mu$ g mL<sup>-1</sup> of collagen overnight in a wet chamber at 4 °C and washed with 0.9% NaCl before use. Collagen fibers covering the channels were visualized by phase contrast microscopy. Human whole blood samples (EFS, Hôpital Bichat, Paris, France) were collected in 75  $\mu$ M PPACK tubes and perfused through the channels for 5–10 min at arterial shear stress (67.5 dyn cm<sup>-2</sup>). Platelet activation and aggregation through contact with collagen in the channels were visualized in real time with phase contrast microscopy (Carl Zeiss Microscopy, Oberkochen, Germany). Channels were washed for 1 min with 0.9% NaCl. To confirm P-selectin expression on platelets, 20  $\mu$ g mL<sup>-1</sup> of FITC anti-CD62P antibody was infused into one channel after platelet aggregation at arterial shear stress for 5 min, and the same concentration of isotype-matched FITC-IgG was injected through the other channel as a control. For binding assay, platelets were labeled with DIOC6 (0.15  $\times$  10<sup>-3</sup> M) before their injection. After platelet aggregation, fluorescent microbubbles (CM-Dextran-RhoB-MBs or Fucoidan-RhoB-MBs) were injected through the channels at 1  $\times$  10<sup>8</sup> mL<sup>-1</sup> for 5 min under venous shear stress (6.75 dyn cm<sup>-2</sup>). Channels were finally washed for 15 min with 0.9% NaCl at the same shear stress. Fluorescence microscopy videos and images were taken along each channel using the same parameters. Quantitative analysis was performed on 7 channels per type of microbubbles. The mean fluorescent intensity of the red fluorescence channel of twenty aggregates was measured using Zen 2012 Software (Carl Zeiss, Oberkochen, Germany).

**In Vitro Ultrasound Imaging:** Ultrasound imaging performances were evaluated with a VisualSonics Vevo<sup>®</sup> 2100 imaging system (FUJIFILM VisualSonics Inc., Canada) connected to a high-frequency transducer (MS550D, VisualSonics). The set-up parameters were: frequency (40 MHz), the acquisition contrast gain (20 dB), the transmit power (4%), the frame rate (33) and the dynamic range (35 dB). All the parameters were constant throughout all image acquisition. A suspension of MBs (10<sup>5</sup> mL<sup>-1</sup>) dispersed into thin-wall PCR tubes was placed on the top of the probe, and the images were obtained by B-mode and linear contrast mode. The burst of microbubbles was performed by using high mechanical index destructive pulse (duration: 1 s). The values of B-mode mean power of 100 frames before and after the destructive pulse were calculated by VevoCQ™ advanced contrast quantification software and shown within the scatter plot. To analyze quantitatively the contrast enhancement effect, the mean values of B-mode power of 100 frames before and after burst were calculated.

**In Vitro Cytotoxicity:** Mouse fibroblast 3T3 cells were cultured in Dulbecco's Modified Eagle Medium (DMEM) supplemented with 10% (v/v) fetal bovine serum, 4 mmol of L-glutamine, 1% (v/v) of penicillin

and 1% (v/v) of streptomycin. The cells were kept in an incubator at 37 °C in a humidified atmosphere of 5% CO<sub>2</sub>, 95% air. Cells were seeded (at the density of 10<sup>4</sup> cells per well) in 96-well plates and incubated for 24 h. The cell culture medium was removed, and 200  $\mu$ L of series of dilution (10<sup>7</sup>, 10<sup>6</sup>, 10<sup>5</sup> and 10<sup>4</sup> mL<sup>-1</sup>) of microbubbles were added in the medium. Culture media were used as a control. After 24 h of incubation, the supernatant was removed, 10  $\mu$ L (5 mg mL<sup>-1</sup>) of MTT solution was added to the medium in each well, and the plates were incubated for 4 h at 37 °C and 5% CO<sub>2</sub>. The medium with MTT was removed, and 100  $\mu$ L per well of isopropanol solution was added to each well to dissolve the formazan crystals. Absorbance was measured immediately using a TECAN (Infinite M200 PRO) at 490 nm. The relative cell viability was expressed as (absorbance of microbubbles/absorbance of the control)  $\times$  100%.

**In Vivo Model of Thrombosis on Rat Deep Vein:** Animal studies were done in accordance with principles of laboratory animal care and with the approval of the animal care and use committee of the Claude Bernard Institute (N°2012-15/698-0100, Paris, France). FeCl<sub>3</sub>-induced thrombosis model on rat deep vein was induced based on the previous work [42]. Briefly, Wistar male rats (Janvier Labs, Le Genest-Saint-Isle, France) aged around 7 weeks were anesthetized with an intraperitoneal injection of pentobarbital (1  $\mu$ L g<sup>-1</sup> body weight, Ceva Santé Animale SA, La Ballastiere, France). A midline abdominal incision was performed to expose the inferior vena cava (IVC). Venous thrombus was generated by applying a 2 mm Whatman chromatography paper saturated with 10% FeCl<sub>3</sub> on top of the IVC in contact with the adventitial surface of the vessel for 5 min. After the paper was removed, the vein was washed several times with a saline solution. Typically, thrombus development was completed 30 min post FeCl<sub>3</sub> injury. Ten thrombosis-bearing rats were randomly divided into two groups, one group of rats received Fucoidan-MBs intracavernous injection (200  $\mu$ L, 1  $\times$  10<sup>8</sup>/mL), the other group was injected with CM-Dextran-MBs (200  $\mu$ L, 1  $\times$  10<sup>8</sup>/mL). As the control, three healthy rats were also injected with Fucoidan-MBs (200  $\mu$ L, 1  $\times$  10<sup>8</sup>/mL). All rats were kept anesthetized during the entire imaging process.

**In Vivo Ultrasound Molecular Imaging:** Ultrasound imaging of venous thrombosis (in rat thrombus model) or venous wall (in healthy rats) was performed using a VisualSonics Vevo<sup>®</sup> 2100 imaging system with the same parameters used *in vitro*. Briefly, the ultrasound transducer was placed perpendicular and parallel to the IVC, 10 min after injection of MBs. A cine loop was acquired in the B-mode and linear contrast mode which made series of imaging frames before and after a high mechanical index destructive pulse (duration: 1 s). Using the Advanced Contrast Quantification Software Analysis Tool (VevoCQ, VisualSonics, Canada), a region of interest (ROI) was defined around the bound MBs area (1 cm<sup>2</sup>). The mean contrast intensity within the ROI before and after the destructive pulse was evaluated, and each data point corresponded to the mean of the contrast intensity in the ROI in each frame. To highlight the contrast effect of targeted MBs, 50 frames after the destructive pulse were selected to create a reference baseline, and the frames before destructive pulse were overlaid to the reference baseline. The system isolated the targeted MBs echo from the tissue ultrasound signal data and identified them in green color. The process persistence filter was set to Smooth (to remove transient bubble data from the image), the contrast overlay dynamic range and threshold were used as default (50%). To analyze quantitatively the contrast enhancement effect, the mean values of contrast power of 200 frames before and after the destructive pulse were calculated by VevoCQ™ advanced contrast quantification software. The signal from the targeted MB was determined by subtracting the mean value after the destructive pulse from the one before. The obtained signal from the targeted MB was normalized to the value before the destructive pulse.

**Histological Evaluations:** Rats were sacrificed with pentobarbital overdose 1 h after injection of Fucoidan-RhoB-MBs. Inferior vena cava with thrombus was removed, washed in 0.9% NaCl, fixed in paraformaldehyde 4% (w/v), and then frozen. The vena samples were

cryosectioned at 10  $\mu\text{m}$  thickness and then stained with hematoxylin and eosin. The cell nuclei of a venous vascular wall were labeled with 4'-6-DiAmidino-2-PhenylIndole (DAPI) contained in mounting medium (Vecto laboratories), and Fucoidan-RhoB-MBs were visualized in red thanks to rhodamine B. Stained sections were observed by light/fluorescence microscopy using the NDPview software (Hamamatsu, Japan). The magnified images of the region of interest were used to show the position of microbubbles.

Biodistribution of Fucoidan-RhoB-MBs was studied in a similar way. Briefly, liver, spleen, lungs, and kidneys were excised and washed at 1 h after injection of Fucoidan-RhoB-MBs. The samples were cryosectioned, cell nuclei were labeled with DAPI, and observed by fluorescence microscopy.

**Statistical Analysis:** All results are presented as the mean  $\pm$  standard deviation (SD). Statistical differences for multiple groups were determined using a one-way ANOVA, and each experiment was performed using Student's t-test. Probabilities of  $p < 0.05$  were considered significant. Statistical analyses were performed using GraphPad Prism 5.0.

### 3. Results and discussion

#### 3.1. Preparation and characterization of microbubbles

Limitations of the first generation of MBs were addressed either by incorporating the echogenic reflective air component into less permeable coatings, such as organic polymers and cross-linked proteins, or by employing less soluble gaseous compounds [43]. Since the first PBCA MBs developed by Harris et al., several antibodies and peptides were employed to produce targeted PBCA MBs with a multi-step synthesis for molecular ultrasound imaging [44]. However, immunogenicity and cost of antibodies limited their use in humans. Moreover, the production of these targeted bubbles is also time-consuming due to their multi-step synthesis (carboxyl groups introduced on the surface through partial hydrolysis of the shell of PBCA MBs [45]). Furthermore, the degree of hydrolysis is difficult to control, and the excess of hydroxyl or redundant reaction time may induce rapid depolymerization reaction destroying the structure of MBs and producing short chains of PBCA [46].

In this work, we reported air-filled PIBCA MBs coated with various polysaccharides in a novel simple one-pot procedure (Fig. 1). The size distribution of MBs before and after polysaccharide functionalization

**Table 1**  
Characteristics of non-functionalized and polysaccharide functionalized microbubbles.

	Size distributions			$\zeta$ (mV)
	D <sub>10</sub> ( $\mu\text{m}$ )	D <sub>50</sub> ( $\mu\text{m}$ )	D <sub>90</sub> ( $\mu\text{m}$ )	
MBs	2.34 $\pm$ 0.01	3.69 $\pm$ 0.01	5.85 $\pm$ 0.01	-15.33 $\pm$ 0.40
Dextran-MBs	2.46 $\pm$ 0.01	3.90 $\pm$ 0.02	6.18 $\pm$ 0.06	-8.56 $\pm$ 0.50
DEAE-Dextran-MBs	2.63 $\pm$ 0.05	4.03 $\pm$ 0.10	6.06 $\pm$ 0.21	44.20 $\pm$ 2.38
CM-Dextran-MBs	2.53 $\pm$ 0.02	4.03 $\pm$ 0.05	6.44 $\pm$ 0.14	-34.33 $\pm$ 0.47
Fucoidan-MBs	2.40 $\pm$ 0.02	3.83 $\pm$ 0.03	6.23 $\pm$ 0.12	-42.80 $\pm$ 1.47

was not altered (Table 1), all MBs showing a single peak with a narrow size distribution (Fig. S1 Left). The surface charge of MBs was similar to the charge of polysaccharides (Table 1 and Fig. S1 Right), indicating that polysaccharides were present at the surface of the MBs [47,48]. Among the polysaccharides, DEAE-Dextran and CM-Dextran could respectively provide amino groups and carboxyl groups on the surface of PIBCA MBs for further functionalization.

Since CM-dextran had a similar negative surface charge but without the sulfate groups of fucoidan that are involved in its interaction with P-selectin, CM-Dextran-MBs were chosen as a control to assess the benefit of using targeted MBs (Fucoidan-MBs). Morphology images of CM-Dextran-MBs and Fucoidan-MBs obtained by electron microscopy showed that all MBs were spherical with an empty core loaded with air (Fig. 2 Left). Under Environmental Scanning Electron Microscopy (ESEM), low vacuum protected the integrity of MBs structure, and both MBs presented similar size by DLS measurement. Fluorophore-labeled MBs in combination with fluorescence microscopy were very powerful tools for clearly visualizing and validating *in vitro* and *in vivo* binding studies. However, the loading strategy should be carefully designed to avoid an alteration of the surface functional groups of MBs. Here, rhodamine-loaded Fucoidan-MBs (Fucoidan-RhoB-MBs) and CM-Dextran-MBs (CM-Dextran-RhoB-MBs) were prepared by modification of the synthesis methods of Liu [49]. The loading of rhodamine into the MBs polymer membrane did not affect the size distribution and zeta potential of MBs. To demonstrate the presence of CM-Dextran or fucoidan on MBs, FITC-CM-Dextran or FITC-fucoidan was added, respectively (Fig. S2). Size distribution and zeta potential of all the

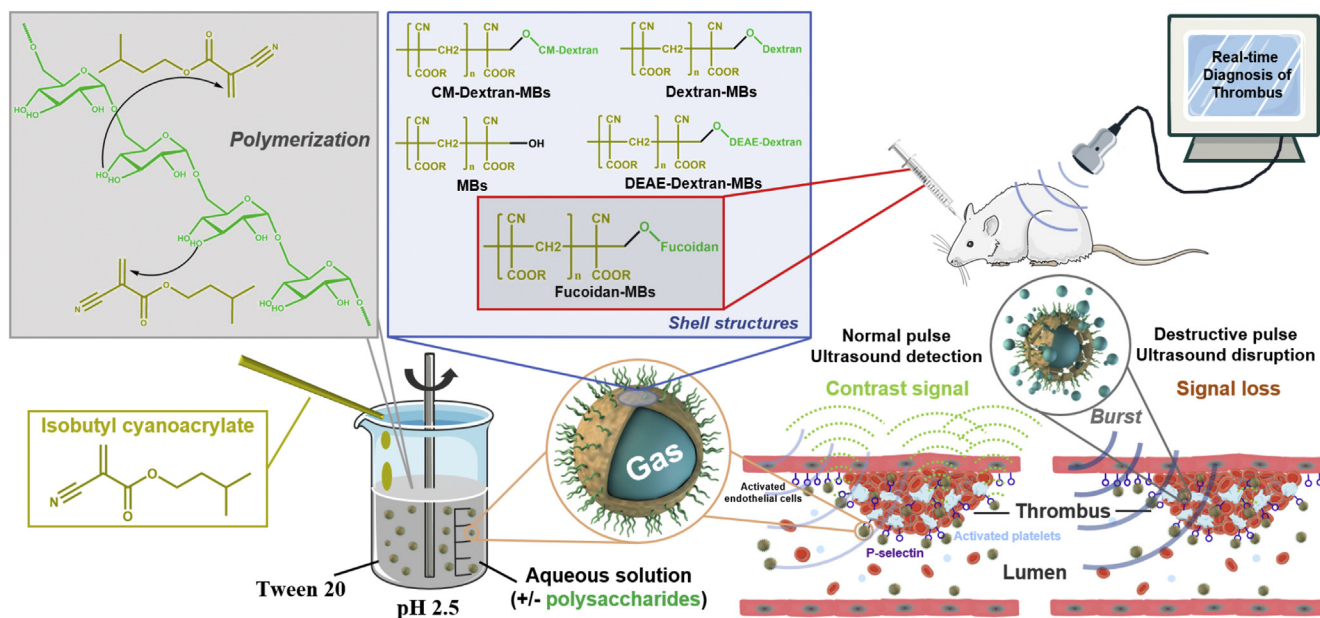


**Fig. 1.** Overall schematic diagram of one-step protocol for microbubbles and their use as molecular ultrasound contrast agent.

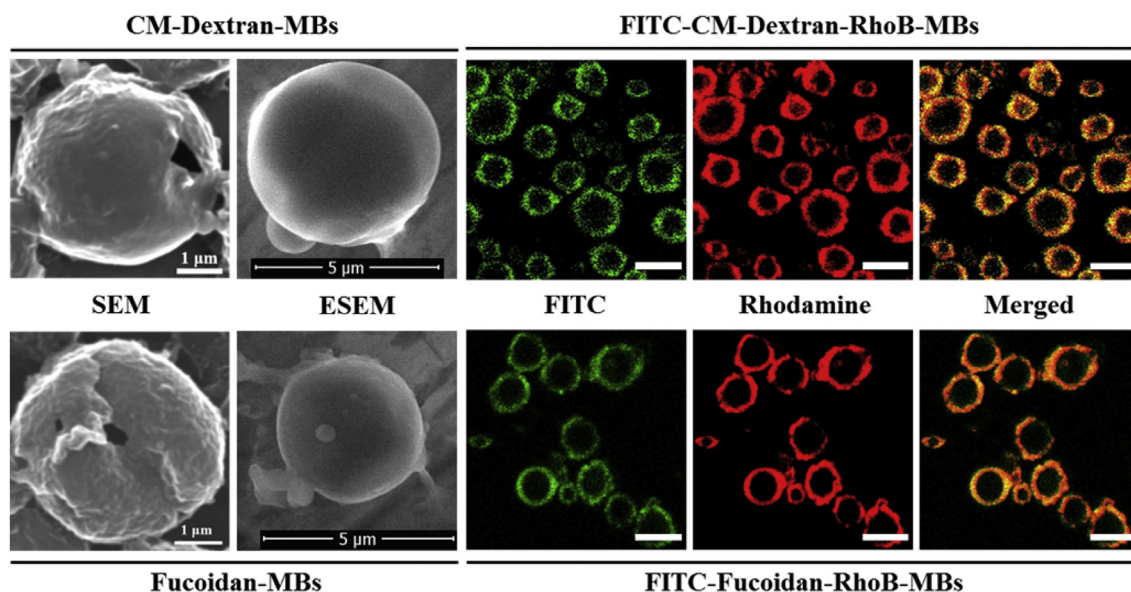


Fig. 2. Morphology characterizations of CM-Dextran-MBs and Fucoïdan-MBs (Left) and fluorescently labeled microbubbles (Right). The green fluorescence signal is from FITC-CM-Dextran or FITC-Fucoïdan, and the red fluorescence signal is from rhodamine (Scale bar for confocal images: 5 μm).

labeled MBs were presented in Table S1. The double-labeled MBs observed by confocal microscopy imaging confirmed the core-shell structure of MBs and the presence of polysaccharides on the shell (Fig. 2 Right).

The amount of fucoïdan coupled to the MBs was quantified by a solid-phase colorimetric assay described by Lee [41]. Based on the standard curves, we calculated the fucoïdan content of Fucoïdan-MBs to be of  $8.6 \times 10^{-15}$  g per Fucoïdan-MB (Fig. S3).

As a potential contrast agent, the storage of MBs is very important. Long-term storage stability of the MBs in aqueous suspensions at 4 °C was evaluated. Results showed that size and zeta potential remained stable for at least 2 months for both MBs (Fig. 3).

### 3.2. In vitro flow experiments

Flow chamber experiments are used to mimic the interactions of MBs with purified P-Selectin or activated human platelets under physiological conditions *in vitro* [36,50]. After perfusion of human whole blood at high shear stress, activated DIOC6 stained human platelets aggregated on collagen-coated chambers. Human platelet aggregates were visualized in real time under the fluorescent microscope (Video S1). P-selectin expression on activated platelets was evidenced by the

green fluorescence uptake observed after injection of FITC-*anti*-CD62P antibody through the channel; no signal was detected after injection of FITC-IgG control (Fig. S4). After perfusion at venous shear stress ( $6.75 \text{ dyn cm}^{-2}$ ) to mimic venous flow conditions of Fucoïdan-RhoB-MBs (Video 1) or CM-Dextran-RhoB-MBs (Video S2) on preformed platelet aggregates, an uptake of red fluorescence was observed over time at the surface of the aggregates. After washing, bound Fucoïdan-RhoB-MBs remained attached to the aggregates, whereas almost no remaining binding was observed with control CM-Dextran-RhoB-MBs (Fig. 4A). Quantitative analysis confirmed that the mean fluorescent intensity (MFI) of fluorescent MBs was significantly higher for Fucoïdan-RhoB-MBs than for CM-Dextran-RhoB-MBs ( $4387 \pm 178.9$  versus  $1640 \pm 10.53$ , respectively,  $p < 0.0001$ ) (Fig. 4B). To further confirm these results, CM-Dextran-RhoB-MBs and Fucoïdan-RhoB-MBs were successively perfused into the same channel at constant shear stress, and the results showed clearly different targeting responses (Video S3).

Supplementary video related to this article can be found at <https://doi.org/10.1016/j.biomaterials.2018.12.023>.

To confirm the binding of Fucoïdan-MBs to activated platelets, we performed an *ex vivo* platelets-rich thrombus and added a suspension of Fucoïdan-MBs for 5 min. After rinsing with saline, we observed the

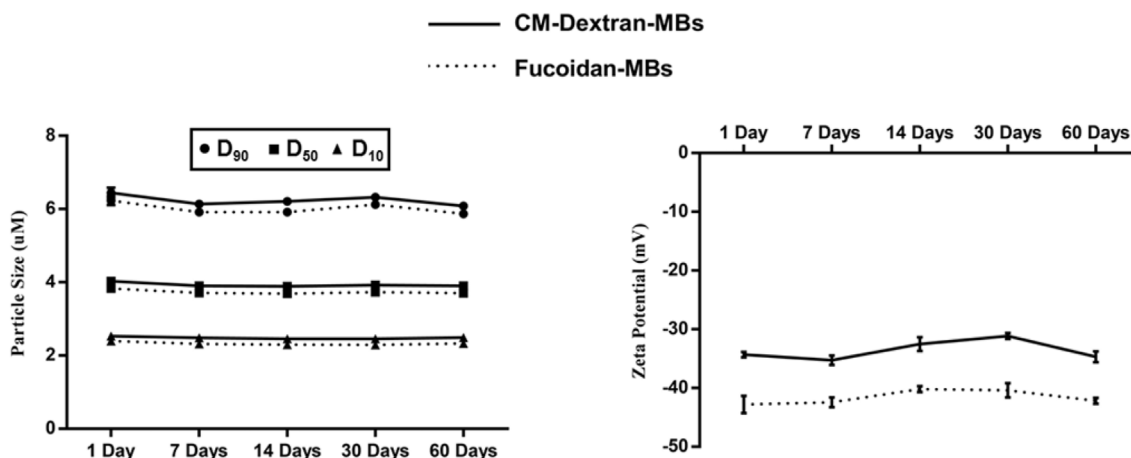
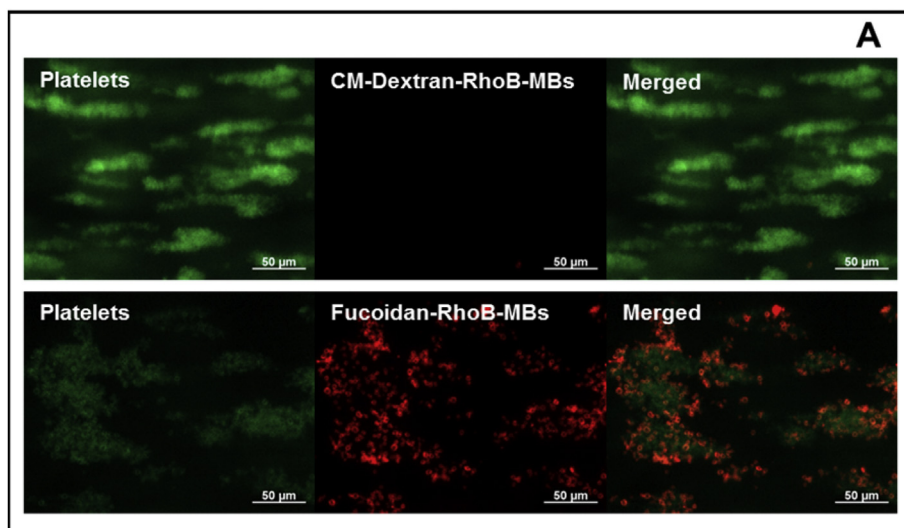
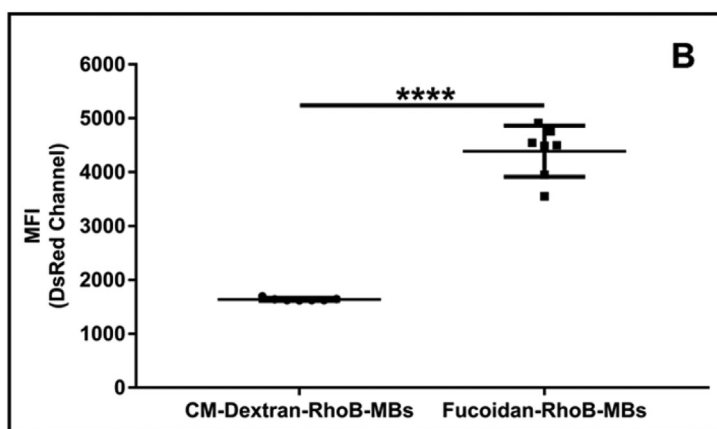


Fig. 3. Stability of size and zeta potential of CM-Dextran-MBs and Fucoïdan-MBs kept at 4 °C for 60 days (n = 3).



**Fig. 4.** Binding of microbubbles on activated platelet aggregates under flow conditions *in vitro*. **A)** Human whole blood labeled with 5  $\mu\text{M}$  of DIOC6 (green) was first injected into channels coated with collagen to induce platelet aggregation (Left panels). Rhodamine labeled CM-Dextran-MBs or Fucoïdan-MBs (red) were infused for 5 min onto activated platelet aggregates under venous flow conditions ( $6.75 \text{ dyn cm}^{-2}$ ). Channels were washed and observed by fluorescent microscopy (middle and right panels). **B)** Quantitative analysis of the mean fluorescent intensity (MFI) on platelet aggregates. One MFI value was obtained per channel on 20 platelet aggregates from 7 independent experiments (\*\*\*\* indicated  $p < 0.0001$ ).



thrombus by Environmental Scanning Electron Microscopy. The ESEM images of the platelets-rich thrombus without MBs exhibited activated platelets and fibrin (Fig. S5 Left). In contrast, the ESEM images of the platelets-rich thrombus in contact with Fucoïdan-MBs showed many spherical micrometer particles (as Fig. 2 Left) associated with the activated platelets confirming that Fucoïdan-MBs bind to activated platelets overexpressing P-selectin.

### 3.3. *In vitro* ultrasound imaging

The potential of CM-Dextran-MBs and Fucoïdan-MBs as contrast agents for ultrasound imaging was first assessed *in vitro*. A suspension of MBs ( $10^5 \text{ mL}^{-1}$ ) was put into the thin-wall tube and placed on the top of the probe (Fig. 5A Left), and the echogenicity of MBs was evaluated by Vevo 2100. A Control suspension was used to check the background signal (Fig. 5A Middle) which remained at low level (Fig. 5A Right). For MBs suspensions, the imaging showed a high and stable enhancement of monodisperse contrast signal, which could be eliminated by destructive pulse (Fig. 5B). Quantitative analysis proved that CM-Dextran-MBs and Fucoïdan-MBs have similar contrast signals and both of them could be reduced to background level after burst (Fig. 5C). These results indicated that the variation in echo after the burst could be used *in vivo* to ensure that the enhanced contrast signal was coming from MBs and not from motion artifact caused by respiratory and cardiac activities.

### 3.4. Cell viability

The cytotoxicity of Fucoïdan-MBs was evaluated by MTT assay [51] with mouse fibroblast 3T3 cells exposed to various concentrations of Fucoïdan-MBs or CM-Dextran-MBs. As shown in Fig. S6, the results demonstrated that none of these MBs affected the cell viability (cell viability  $> 80\%$  even at the highest concentrations of  $10^7 \text{ mL}^{-1}$ ), suggesting an excellent *in vitro* safety of these MBs. Moreover, no significant difference was observed between CM-Dextran-MBs and Fucoïdan-MBs.

### 3.5. *In vivo* ultrasound imaging and Environmental Scanning Electron Microscopy

To evaluate the *in vivo* targeting of Fucoïdan-MBs to P-selectin overexpressed on thrombus, the ferric chloride ( $\text{FeCl}_3$ ) induced inferior vena cava (IVC) non-occlusive thrombus rat model was performed. The presence of non-occlusive thrombus was inspected by B-mode, and the venous blood flow around thrombi was confirmed by Color Doppler Flow Imaging (Fig. S7). Ten minutes after the injection of Fucoïdan-MBs, the presence of bound Fucoïdan-MBs in the thrombus region was accurately validated (green color) (Video 2). The signal intensity of binding area in the thrombus was remarkably decreased after MBs burst by destructive pulse (Fig. 6B). In contrast, the rats injected with control CM-Dextran-MBs showed few MBs in the thrombus region (Video S4), and the signal intensity declined only slightly after the destructive pulse (Fig. 6A). Subsequent quantifications of the decreased signal intensity in the thrombus area before and after destructive pulse evidenced a

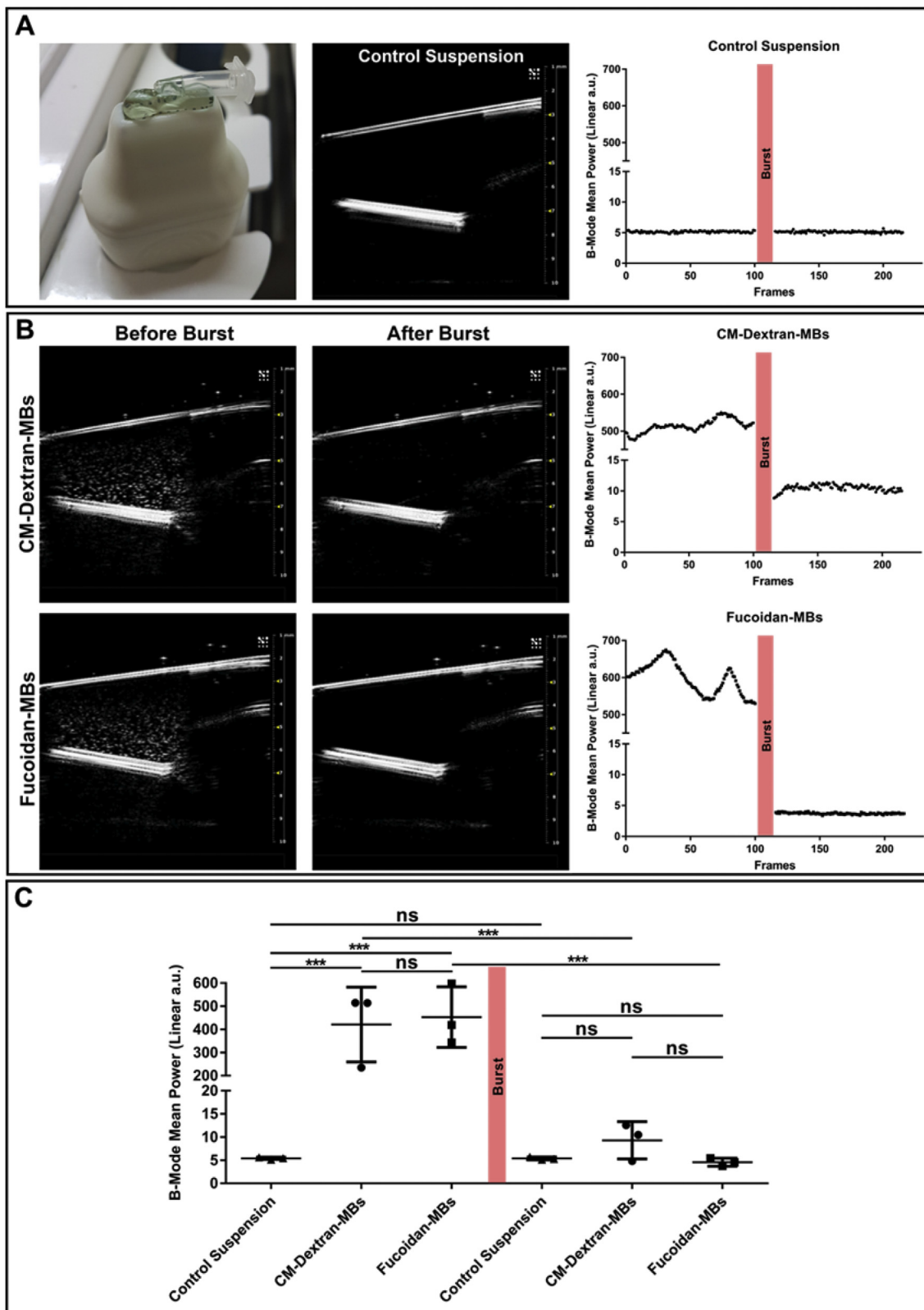


**Fig. 5.** *In vitro* ultrasound signals of CM-Dextran-MBs and Fucoidan-MBs under B-mode. **A**) Image of the experimental set-up (Left); The control suspension of MBs shows the baseline signal (Middle); The B-mode mean power of 100 frames before and after high mechanical destructive pulse were calculated by VevoCQ™ and displayed by scatter plot (Right). **B**) Visualization of the contrast intensities before and after the burst to destroy CM-Dextran-MBs (Up) and Fucoidan-MBs (Down). **C**) Quantitative analysis of the B-mode mean power signals before and after the burst. (n = 3; ns: non-significant; \*\*\*p < 0.001).

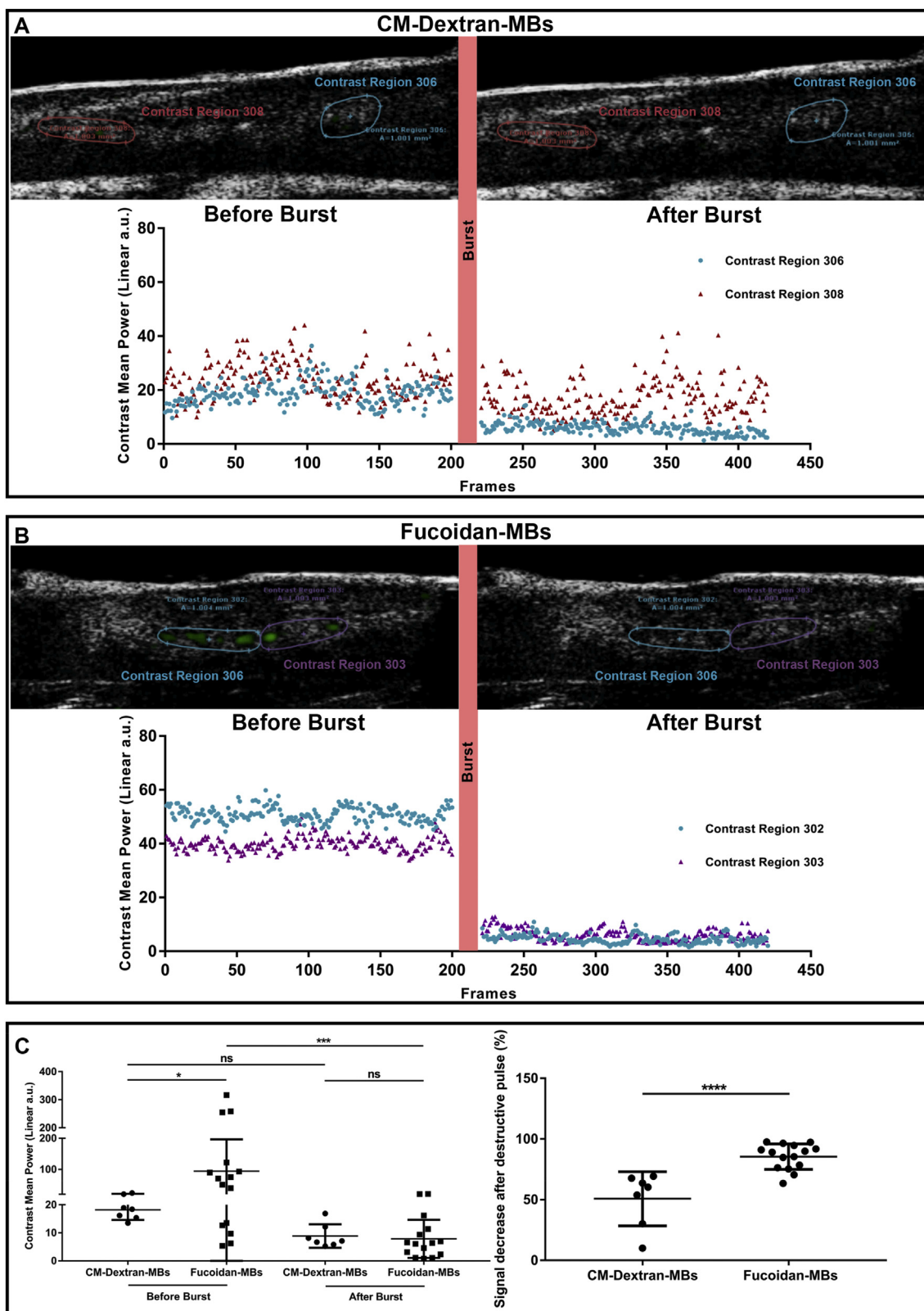


**Fig. 6.** The thrombus area ultrasound imaging of ferric-chloride-induced inferior vena cava thrombosis rat model was acquired and analyzed for 10 min after injection of MBs. 50 frames after the destructive pulse were selected as a reference, and the contrast signals that only exist in the frame before burst were highlighted by green color. The contrast mean power of 200 frames before and after high mechanical destructive pulse was calculated by VevoCQ™ and represented in scatter plot. The mean value of contrast mean power before and after the burst was used for the following quantitative analyses. **A)** After injection of CM-Dextran-MBs, few bound MBs were found in thrombus region. **B)** A significant microbubble-induced signal (green) was present in the thrombus area after injection of Fucoidan-MBs. **C)** Quantitative analysis of the signals before and after the burst. On the right panel, the contrast mean power after the burst was normalized to the one before the burst (5 rats for CM-Dextran-MBs and 5 rats for Fucoidan-MBs, \*\*\*\*p < 0.0001).

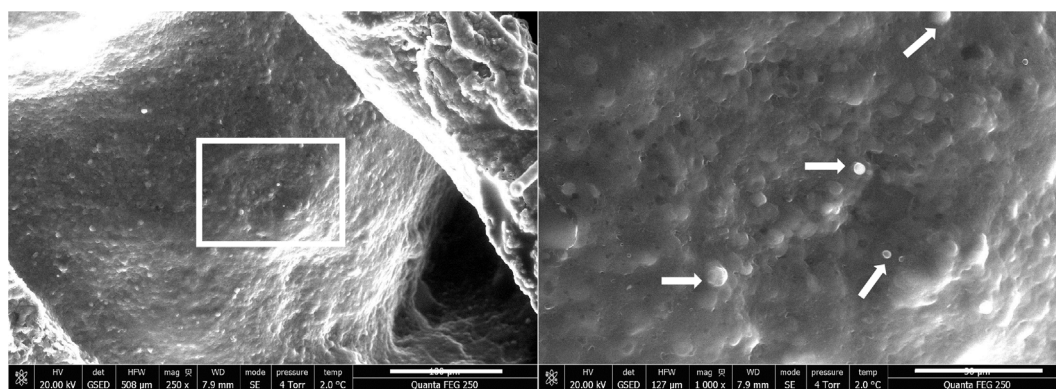


**Fig. 7.** Environmental Scanning Electron Microscopy (ESEM) images of a non-occlusive inferior vena cava thrombus rat model with Fucoïdan-MBs bound at the luminal surface of the thrombus (Left). Magnification of a region of interest and white arrows highlight the Fucoïdan-MBs (Right). Scale bars are 100  $\mu\text{m}$  and 30  $\mu\text{m}$  for the magnified area.

significantly higher accumulation of Fucoïdan-MBs in comparison to CM-Dextran-MBs ( $85.5 \pm 2.7\%$  versus  $50.8 \pm 8.4\%$ , respectively,  $p < 0.0001$ ) (Fig. 6C). Furthermore, no Fucoïdan-MBs were detected in the inferior vein wall of healthy rats (Fig. S8). In addition, the healthy rats used in these experiments were still alive a few months after injection of MBs and without any side effects.

Supplementary video related to this article can be found at <https://doi.org/10.1016/j.biomaterials.2018.12.023>.

To confirm the presence of Fucoïdan-MBs bound onto the thrombus, we visualized the opened inferior vena cava vein with thrombus by Environmental Scanning Electron Microscopy (ESEM). ESEM images proved that the thrombus rat model induced by ferric chloride ( $\text{FeCl}_3$ ) was non-occlusive (Fig. 7 Left) and that there were many Fucoïdan-MBs at the luminal surface of the thrombus targeting the P-selectin over-expressed (Fig. 7 Right).

Owing to the poor contrast, quantitative analysis of ultrasound signal modification has been a difficult issue in the field of ultrasound molecular imaging [42,52,53]. Unlike non-motile solid tumor, blood vessel walls are always dilated or contracted due to the heartbeat, adding to the difficulty of thrombi imaging analysis. Currently, the main ultrasound imaging methods of thrombus analysis are based on the contrast overlay data that is created by comparing the imaging before and after the injection of MBs [42,52,53]. This approach could potentially overcome the interference of motion artifacts, but it failed to distinguish the false increased contrast signal caused by the growth of thrombi. Herein, we exploited a differential imaging method to evaluate the targeting efficiency of MBs. Thanks to this method, we were able to distinctly see the binding site of MBs, quantify the number of targeted MBs, and also monitor the elimination of MBs. Previous studies have shown that the combination of MBs and ultrasound can help temporarily to open the blood-brain-barrier via sonoporation mechanisms, these phenomena can contribute to the delivery of pharmaceutical treatments [54–57]. Herein, we observed for the first time that Fucoïdan-MBs which were localized in the thrombus could be destroyed by a destructive pulse. These results indicated that Fucoïdan-MBs carrying thrombolytic drugs could be a promising delivery system to improve thrombolytic efficiency while reducing hemorrhagic complications via the local release of the drug-loaded Fucoïdan-MBs at the pathological site.

### 3.6. Tissue distribution in healthy and thrombus-induced rats

To evaluate the biodistribution in healthy rats, the presence of Fucoïdan-RhoB-MBs in four main organs of excretion (liver, spleen, lungs and kidneys) was assessed by histological analysis of several sections for each organ (Fig. S9). Results revealed that few Fucoïdan-RhoB-MBs were found in liver, lungs and kidneys (indicated by the

arrows). Conversely, red fluorescence was detected in the spleen with irregular shapes probably due to the degradation of the microbubbles. Indeed, various degradation processes of PACA nanoparticles were described [58,59]. One leading view was that the main products of biodegradation of PACA nanoparticles were polymer chains and the corresponding alcohol, which were formed after cleavage of ester bond by esterases [60–62]. This also confirmed that the red fluorescent fragments we observed possibly arise from enzymatic hydrolysis in the spleen. Considering the results of the absence of cell toxicity and the low injection doses of Fucoïdan-MBs or CM-Dextran-MBs *in vivo*, these MBs seem to be safe.

To assess whether Fucoïdan-MBs accumulated *in vivo* within an inferior venous thrombus, histology was performed under bright field and fluorescent microscopes. Results confirmed that thrombus existed in the inferior deep vein (Fig. 8A), smooth muscle cells from venous vascular wall labeled with DAPI showed blue color (Fig. 8B), and many scattered Fucoïdan-RhoB-MBs (indicated by the arrows) were localized in the thrombus area (Fig. 8C and D). Few MBs showed microbubble-like shapes, most of them were altered and fractured (Fig. 8C and D Right), likely due to high destructive pulse that destroyed their structure.

## 4. Conclusion

In this work, various polysaccharide-coated PIBCA MBs were developed according to a new easy one-step polymerization reaction. This method allowed convenient modulation of the different surface functional groups of MBs, which were prone to further functionalization. Among the polysaccharides, fucoidan was especially considered to functionalize the MBs due to its high affinity for P-selectin. Compared to anionic carboxymethylated dextran MBs, Fucoïdan-MBs specifically bind to P-selectin expressed by human activated platelets at venous shear stress. An *in vivo* rat model showed that Fucoïdan-MBs were able to target thrombus. We evidenced their presence in the thrombus by ultrasound imaging and histology analysis. This approach offers a sensitive and specific method to detect microthrombi before complete occlusion of the vessel using an inexpensive and widely used ultrasound equipment in hospitals and medical centers worldwide. Fucoïdan-MBs application could also be extended to molecular monitoring of P-selectin expression in severe diseases. More in-depth studies of the *in vivo* performance of Fucoïdan-MBs should be performed before moving towards clinical implementation. In addition, antithrombotic or fibrinolytic drugs could be incorporated into the Fucoïdan-MBs, and these targeted MBs burst by ultrasound could locally deliver the drugs at the thrombus site, which represents a new promising theranostic system.

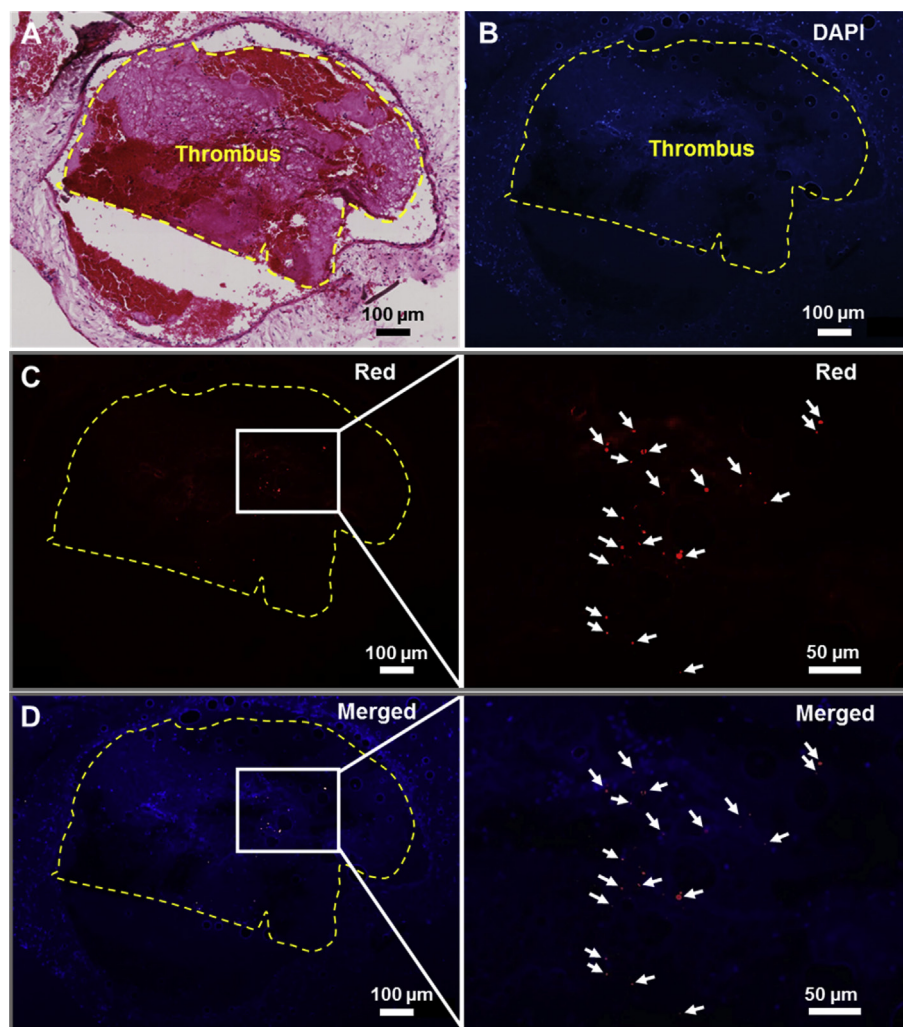


**Fig. 8.** Histological analysis of thrombi in the IVC sections. Hematoxylin and Eosin staining (A) and DAPI staining (B). Red Fucoidan-RhoB-MBs were only observed in the thrombus area (C). Merge section of DAPI and Fucoidan-RhoB-MBs (D). Inserts are magnification of Regions of Interest (C & D Right). The region of thrombus is denoted with the yellow dotted line.

#### Data availability statement

Authors confirm that the raw/processed data required to reproduce these findings can be shared upon demand.

#### Acknowledgements

This study was supported by Inserm, Paris Diderot University, and Paris 13 University. Dr. B. Li is a recipient of the China Scholarship Council (CSC, No. 201206180031), he designed the study, collected and interpreted the data, and wrote the draft version of the manuscript. R. Aid-Launais (Engineer) carried out the rat experiment, histology and cytotoxicity analysis. Dr. M-N. Labour (Post-Doc) performed the confocal imaging. A. Zenych (PhD student), a recipient of the European Union's Horizon 2020 research and innovation programme (Marie Skłodowska-Curie grant # 665850), realized the physico-chemical characterizations of the MBs and M. Juenet (PhD student) the characterization of fucoidan content. C. Choqueux (Engineer) designed and performed the Environmental Scanning Electron Microscopy experiments. V. Ollivier (Engineer) designed the flow experiments. D. Letourneur (Head of the Unit) provided the funding, discussed the results and corrected the manuscript. O. Couture (Researcher) analyzed the *in vitro* and *in vivo* ultrasound imaging. C. Chauvierre (Researcher) supervised the thesis of Bo Li, discussed the results and corrected the

manuscript. The authors are most grateful to E. Teston (INSERM U979) for *in vitro* ultrasound imaging experiment on agarose, F. Nadaud (UTC Compiègne, France) for ESEM images and to CRI U1149 imaging facilities for confocal imaging. This work received the financial support of the ANR (ANR-12-EMMA-0020-01 “MicroSound” and ANR-13-LAB1-0005-01 “FucoChem”), and the EU project FP7-NMP-2012-LARGE-6-309820 “NanoAthero”. The authors have declared that no competing interest exists.

#### Appendix A. Supplementary data

Supplementary data to this article can be found online at <https://doi.org/10.1016/j.biomaterials.2018.12.023>.

#### References

- [1] N. Mackman, Triggers, targets and treatments for thrombosis, *Nature* 451 (7181) (2008) 914–918.
- [2] G. Lippi, M. Franchini, G. Targher, Arterial thrombus formation in cardiovascular disease, *Nat. Rev. Cardiol.* 8 (9) (2011) 502–512.
- [3] S.P. Jackson, Arterial thrombosis—insidious, unpredictable and deadly, *Nat. Med.* 17 (11) (2011) 1423–1436.
- [4] R.P. Choudhury, V. Fuster, Z.A. Fayad, Molecular, cellular and functional imaging of atherothrombosis, *Nat. Rev. Drug Discov.* 3 (11) (2004) 913–925.
- [5] S. Yokoyama, H. Ikeda, N. Haramaki, H. Yasukawa, T. Murohara, T. Imaizumi, Platelet P-selectin plays an important role in arterial thrombogenesis by forming large stable platelet-leukocyte aggregates, *J. Am. Coll. Cardiol.* 45 (8) (2005)

- 1280–1286.
- [6] H.H. Boersma, H.J. de Haas, C.P. Reutelingsperger, R.H. Slart, P-selectin imaging in cardiovascular disease: what you see is what you get? *J. Nucl. Med.* 52 (9) (2011) 1337–1338.
  - [7] J.K. Schaefer, B. Jacobs, T.W. Wakefield, S.L. Sood, New biomarkers and imaging approaches for the diagnosis of deep venous thrombosis, *Curr. Opin. Hematol.* 24 (3) (2017) 274–281.
  - [8] J. Brangsch, C. Reimann, F. Colletini, R. Buchert, R.M. Botnar, M.R. Makowski, Molecular imaging of abdominal aortic aneurysms, *Trends Mol. Med.* 23 (2) (2017) 150–164.
  - [9] L. Bachelet, I. Bertholon, D. Lavigne, R. Vassy, M. Jandrot-Perrus, F. Chaubet, D. Letourneur, Affinity of low molecular weight fucoidan for P-selectin triggers its binding to activated human platelets, *Biochim. Biophys. Acta* 1790 (2) (2009) 141–146.
  - [10] A.K. Silva, D. Letourneur, C. Chauvierre, Polysaccharide nanosystems for future progress in cardiovascular pathologies, *Theranostics* 4 (6) (2014) 579–591.
  - [11] F. Rouzet, L. Bachelet-Violette, J.M. Alsac, M. Suzuki, A. Meulemans, L. Louedec, A. Petiet, M. Jandrot-Perrus, F. Chaubet, J.B. Michel, D. Le Guludec, D. Letourneur, Radiolabeled fucoidan as a p-selectin targeting agent for in vivo imaging of platelet-rich thrombus and endothelial activation, *J. Nucl. Med.* 52 (9) (2011) 1433–1440.
  - [12] P. Saboural, F. Chaubet, F. Rouzet, F. Al-Shoukr, R.B. Azzouna, N. Bouchemal, L. Picton, L. Louedec, M. Maire, L. Rolland, G. Potier, D.L. Guludec, D. Letourneur, C. Chauvierre, Purification of a low molecular weight fucoidan for SPECT molecular imaging of myocardial infarction, *Mar. Drugs* 12 (9) (2014) 4851–4867.
  - [13] B. Li, M. Juenet, R. Aid-Launais, M. Maire, V. Ollivier, D. Letourneur, C. Chauvierre, Development of polymer microcapsules functionalized with fucoidan to target P-selectin overexpressed in cardiovascular diseases, *Adv. Healthc. Mater.* 6 (4) (2017) 1601200.
  - [14] M. Suzuki, L. Bachelet-Violette, F. Rouzet, A. Beilvert, G. Autret, M. Maire, C. Menager, L. Louedec, C. Choqueux, P. Saboural, O. Haddad, C. Chauvierre, F. Chaubet, J.B. Michel, J.M. Serfaty, D. Letourneur, Ultrasmall superparamagnetic iron oxide nanoparticles coated with fucoidan for molecular MRI of intraluminal thrombus, *Nanomedicine* 10 (1) (2015) 73–87.
  - [15] T. Bonnard, G. Yang, A. Petiet, V. Ollivier, O. Haddad, D. Arnaud, L. Louedec, L. Bachelet-Violette, S.M. Derkaoui, D. Letourneur, C. Chauvierre, C. Le Visage, Abdominal aortic aneurysms targeted by functionalized polysaccharide microparticles: a new tool for SPECT imaging, *Theranostics* 4 (6) (2014) 592–603.
  - [16] T. Bonnard, J.M. Serfaty, C. Journe, B. Ho Tin Noe, D. Arnaud, L. Louedec, S.M. Derkaoui, D. Letourneur, C. Chauvierre, C. Le Visage, Leukocyte mimetic polysaccharide microparticles tracked in vivo on activated endothelium and in abdominal aortic aneurysm, *Acta Biomater.* 10 (8) (2014) 3535–3545.
  - [17] P. Emilia, T. Nicolas, G. Belfor, S. Mathieu, B. Romain, T. Nicolas, K. Erol, L. Olivier, O. Michèle, D.B. Thuy, B.J. Claude, G. Brigitte, U. Wladimir, B.S. Lori, F. Elias, Perfluorooctyl bromide polymeric capsules as dual contrast agents for ultrasonography and magnetic resonance imaging, *Adv. Funct. Mater.* 18 (19) (2008) 2963–2971.
  - [18] R.H. Perera, C. Hernandez, H. Zhou, P. Kota, A. Burke, A.A. Exner, Ultrasound imaging beyond the vasculature with new generation contrast agents, *Rev. Nanomed. Nanobiotechnol.* 7 (4) (2015) 593–608.
  - [19] E. Stride, N. Saffari, Microbubble ultrasound contrast agents: a review, *Proc. Inst. Mech. Eng. H* 217 (6) (2003) 429–447.
  - [20] D. Cosgrove, Ultrasound contrast agents: an overview, *Eur. J. Radiol.* 60 (3) (2006) 324–330.
  - [21] R. Gessner, P.A. Dayton, Advances in molecular imaging with ultrasound, *Mol. Imag.* 9 (3) (2010) 117–127.
  - [22] F. Kiessling, S. Fokong, P. Koczera, W. Lederle, T. Lammers, Ultrasound microbubbles for molecular diagnosis, therapy, and theranostics, *J. Nucl. Med.* 53 (3) (2012) 345–348.
  - [23] J. Wang, P. Li, R. Tian, W. Hu, Y. Zhang, P. Yuan, Y. Tang, Y. Jia, L. Zhang, A novel microbubble capable of ultrasound-triggered release of drug-loaded nanoparticles, *J. Biomed. Nanotechnol.* 12 (3) (2016) 516–524.
  - [24] C. Huang, H. Zhang, R. Bai, Advances in ultrasound-targeted microbubble-mediated gene therapy for liver fibrosis, *Acta Pharm. Sin.* B 7 (4) (2017) 447–452.
  - [25] X. Xiong, F. Zhao, M. Shi, H. Yang, Y. Liu, Polymeric microbubbles for ultrasonic molecular imaging and targeted therapeutics, *Journal of biomaterials science, Polymer Ed.* 22 (4–6) (2011) 417–428.
  - [26] J. Liao, C. Wang, Y. Wang, F. Luo, Z. Qian, Recent advances in formation, properties, and applications of polymerosomes, *Curr. Pharmaceut. Des.* 18 (23) (2012) 3432–3441.
  - [27] C. Vauthier, C. Dubernet, E. Fattal, H. Pinto-Alphandary, P. Couvreur, Poly(alkylcyanoacrylates) as biodegradable materials for biomedical applications, *Adv. Drug Deliv. Rev.* 55 (4) (2003) 519–548.
  - [28] V. Delplace, J. Nicolas, Degradable vinyl polymers for biomedical applications, *Nat. Chem.* 7 (2015) 771.
  - [29] M.D. Stein, D. Heldmann, T.D. Fritzsche, J.D. Siegert, G.D. Rössling, U.P. Speck, *Ultrasound Imaging Agents, Process for Their Preparation and Their Diagnostic and Therapeutic Use*, Google Patents, 1989.
  - [30] J.R. Harris, F. Depoix, K. Ulrich, The structure of gas-filled n-butyl-2-cyanoacrylate (BCA) polymer particles, *Micron* 26 (2) (1995) 103–111.
  - [31] M. Palmowski, J. Huppert, P. Hauff, M. Reinhardt, K. Schreiner, M.A. Socher, P. Hallscheidt, G.W. Kauffmann, W. Semmler, F. Kiessling, Vessel fractions in tumor xenografts depicted by flow- or contrast-sensitive three-dimensional high-frequency Doppler ultrasound respond differently to antiangiogenic treatment, *Canc. Res.* 68 (17) (2008) 7042–7049.
  - [32] M. Palmowski, J. Huppert, G. Ladewig, P. Hauff, M. Reinhardt, M.M. Mueller, E.C. Woenne, J.W. Jenne, M. Maurer, G.W. Kauffmann, W. Semmler, F. Kiessling, Molecular profiling of angiogenesis with targeted ultrasound imaging: early assessment of antiangiogenic therapy effects, *Mol. Canc. Therapeut.* 7 (1) (2008) 101–109.
  - [33] M. Palmowski, B. Morgenstern, P. Hauff, M. Reinhardt, J. Huppert, M. Maurer, E.C. Woenne, S. Doerk, G. Ladewig, J.W. Jenne, S. Delorme, L. Grenacher, P. Hallscheidt, G.W. Kauffmann, W. Semmler, F. Kiessling, Pharmacodynamics of streptavidin-coated cyanoacrylate microbubbles designed for molecular ultrasound imaging, *Invest. Radiol.* 43 (3) (2008) 162–169.
  - [34] P. Koczera, Z. Wu, S. Fokong, B. Theek, L. Appold, S. Jorge, D. Mockel, Z. Liu, A. Curaj, G. Storm, M. van Zandvoort, F. Kiessling, T. Lammers, Fluorescently labeled microbubbles for facilitating translational molecular ultrasound studies, *Drug Deliv. Transl. Res.* 2 (1) (2012) 56–64.
  - [35] S. Fokong, B. Theek, Z. Wu, P. Koczera, L. Appold, S. Jorge, U. Resch-Genger, M. van Zandvoort, G. Storm, F. Kiessling, T. Lammers, Image-guided, targeted and triggered drug delivery to tumors using polymer-based microbubbles, *J. Contr. Release* 163 (1) (2012) 75–81.
  - [36] Z. Wu, A. Curaj, S. Fokong, E.A. Liehn, C. Weber, T. Lammers, F. Kiessling, M. Zandvoort van, Rhodamine-loaded intercellular adhesion molecule-1-targeted microbubbles for dual-modality imaging under controlled shear stresses, *Circ. Cardiovasc. Imag.* 6 (6) (2013) 974–981.
  - [37] S. Fokong, A. Fragoso, A. Rix, A. Curaj, Z. Wu, W. Lederle, O. Iranzo, J. Gatjens, F. Kiessling, M. Palmowski, Ultrasound molecular imaging of E-selectin in tumor vessels using poly n-butyl cyanoacrylate microbubbles covalently coupled to a short targeting peptide, *Invest. Radiol.* 48 (12) (2013) 843–850.
  - [38] I. Spivak, A. Rix, G. Schmitz, S. Fokong, O. Iranzo, W. Lederle, F. Kiessling, Low-dose molecular ultrasound imaging with E-selectin-targeted PBCA microbubbles, *Mol. Imag. Biol.* 18 (2) (2016) 180–190.
  - [39] M. Smeenge, F. Tranquart, C.K. Nanaerts, T.M. de Reijke, M.J. van de Vijver, M.P. Laguna, S. Pochon, J. de la Rosette, H. Wijkstra, First-in-human ultrasound molecular imaging with a VEGFR2-specific ultrasound molecular contrast agent (BR55) in prostate cancer: a safety and feasibility pilot study, *Invest. Radiol.* 52 (7) (2017) 419–427.
  - [40] J.K. Willmann, L. Bonomo, A. Carla Testa, P. Rinaldi, G. Rindi, K.S. Valluru, G. Petrone, M. Martini, A.M. Lutz, S.S. Gambhir, Ultrasound molecular imaging with BR55 in patients with breast and ovarian lesions: first-in-human results, *J. Clin. Oncol.* 35 (19) (2017) 2133–2140.
  - [41] J.M. Lee, Z.-U. Shin, G.T. Mavlonov, I.Y. Abdurakhmonov, T.H. Yi, Solid-phase colorimetric method for the quantification of fucoidan, *Appl. Biochem. Biotechnol.* 168 (5) (2012) 1019–1024.
  - [42] T. Wang, C. Yuan, B. Dai, Y. Liu, M. Li, Z. Feng, Q. Jiang, Z. Xu, N. Zhao, N. Gu, F. Yang, Click-chemistry-mediated rapid microbubble capture for acute thrombus ultrasound molecular imaging, *ChemBiochem* 18 (14) (2017) 1364–1368.
  - [43] N. Guvener, L. Appold, F. de Lorenzi, S.K. Golombek, L.Y. Rizzo, T. Lammers, F. Kiessling, Recent advances in ultrasound-based diagnosis and therapy with micro- and nanometer-sized formulations, *Methods* 130 (2017) 4–13.
  - [44] A. Curaj, Z. Wu, A. Rix, O. Gresch, M. Sternkopf, S. Alampour-Rajabi, T. Lammers, M. van Zandvoort, C. Weber, R.R. Koenen, E.A. Liehn, F. Kiessling, Molecular ultrasound imaging of junctional adhesion molecule depicts acute alterations in blood flow and early endothelial dysregulation, *Arterioscler. Thromb. Vasc. Biol.* 38 (1) (2018) 40–48.
  - [45] P. Koczera, L. Appold, Y. Shi, M. Liu, A. Dasgupta, V. Pathak, T. Ojha, S. Fokong, Z. Wu, M. van Zandvoort, O. Iranzo, A.J.C. Kuehne, A. Pich, F. Kiessling, T. Lammers, PBCA-based polymeric microbubbles for molecular imaging and drug delivery, *J. Contr. Release* 259 (2017) 128–135.
  - [46] B. Ryan, G. McCann, Novel sub-ceiling temperature rapid depolymerization-repolymerization reactions of cyanoacrylate polymers, *Macromol. Rapid Commun.* 17 (4) (1996) 217–227.
  - [47] C. Chauvierre, D. Labarre, P. Couvreur, C. Vauthier, Novel polysaccharide-decorated poly(isobutyl cyanoacrylate) nanoparticles, *Pharm. Res.* 20 (11) (2003) 1786–1793.
  - [48] C. Chauvierre, C. Vauthier, D. Labarre, P. Couvreur, M.C. Marden, L. Leclerc, A new generation of polymer nanoparticles for drug delivery, *Cell. Mol. Biol.* 50 (3) (2004) 233–239.
  - [49] Z. Liu, P. Koczera, D. Doleschel, F. Kiessling, J. Gatjens, Versatile synthetic strategies for PBCA-based hybrid fluorescent microbubbles and their potential theranostic applications to cell labelling and imaging, *Chem. Commun.* 48 (42) (2012) 5142–5144.
  - [50] W. Wu, Y. Wang, S. Shen, J. Wu, S. Guo, L. Su, F. Hou, Z. Wang, Y. Liao, J. Bin, In vivo ultrasound molecular imaging of inflammatory thrombosis in arteries with cyclic Arg-Gly-asp-modified microbubbles targeted to glycoprotein IIb/IIIa, *Invest. Radiol.* 48 (11) (2013) 803–812.
  - [51] J. Matuszak, J. Baumgartner, J. Zaloga, M. Juenet, A.E. da Silva, D. Franke, G. Almer, I. Texier, D. Faivre, J.M. Metselaar, F.P. Navarro, C. Chauvierre, R. Prassl, L. Dezi, R. Urbanics, C. Alexiou, H. Mänge, J. Szeben, D. Letourneur, I. Cicha, Nanoparticles for intravascular applications: physicochemical characterization and cytotoxicity testing, *Nanomedicine* 11 (6) (2016) 597–616.
  - [52] X. Wang, C.E. Hagemeyer, J.D. Hohmann, E. Leitner, P.C. Armstrong, F. Jia, M. Olschewski, A. Needles, K. Peter, I. Ahrens, Novel single-chain antibody-targeted microbubbles for molecular ultrasound imaging of thrombosis: validation of a unique noninvasive method for rapid and sensitive detection of thrombi and monitoring of success or failure of thrombolysis in mice, *Circulation* 125 (25) (2012) 3117–3126.
  - [53] X. Wang, Y. Gkanatsas, J. Palasubramaniam, J.D. Hohmann, Y.C. Chen, B. Lim, C.E. Hagemeyer, K. Peter, Thrombus-targeted theranostic microbubbles: a new technology towards concurrent rapid ultrasound diagnosis and bleeding-free fibrinolytic treatment of thrombosis, *Theranostics* 6 (5) (2016) 726–738.

- [54] M.A. Nakatsuka, R.F. Mattrey, S.C. Esener, J.N. Cha, A.P. Goodwin, Aptamer-crosslinked microbubbles: smart contrast agents for thrombin-activated ultrasound imaging, *Adv. Mater.* 24 (45) (2012) 6010–6016.
- [55] E. Unger, T. Porter, J. Lindner, P. Grayburn, Cardiovascular drug delivery with ultrasound and microbubbles, *Adv. Drug Deliv. Rev.* 72 (2014) 110–126.
- [56] T. Lammers, P. Koczera, S. Fokong, F. Gremse, J. Ehling, M. Vogt, A. Pich, G. Storm, M. van Zandvoort, F. Kiessling, Theranostic USPIO-loaded microbubbles for mediating and monitoring blood-brain barrier permeation, *Adv. Funct. Mater.* 25 (1) (2015) 36–43.
- [57] C.H. Fan, C.Y. Lin, H.L. Liu, C.K. Yeh, Ultrasound targeted CNS gene delivery for Parkinson's disease treatment, *J. Contr. Release* 261 (2017) 246–262.
- [58] V. Lenaerts, P. Couvreur, D. Christiaens-Leyh, E. Joiris, M. Roland, B. Rollman, P. Speiser, Degradation of poly (isobutyl cyanoacrylate) nanoparticles, *Biomaterials* 5 (2) (1984) 65–68.
- [59] R.H. Muller, C. Lherm, J. Herbort, P. Couvreur, In vitro model for the degradation of alkylcyanoacrylate nanoparticles, *Biomaterials* 11 (8) (1990) 590–595.
- [60] M. Stein, E. Hamacher, Degradation of polybutyl 2-cyanoacrylate microparticles, *Int. J. Pharm.* 80 (1) (1992) R11–R13.
- [61] D. Scherer, J.R. Robinson, J. Kreuter, Influence of enzymes on the stability of polybutylcyanoacrylate nanoparticles, *Int. J. Pharm.* 101 (1) (1994) 165–168.
- [62] C. O'Sullivan, C. Birkinshaw, Hydrolysis of poly (n-butylcyanoacrylate) nanoparticles using esterase, *Polym. Degrad. Stabil.* 78 (1) (2002) 7–15.